

PREPARED FOR THE U.S. DEPARTMENT OF ENERGY,
UNDER CONTRACT DE-AC02-76CH03073

PPPL-3875
UC-70

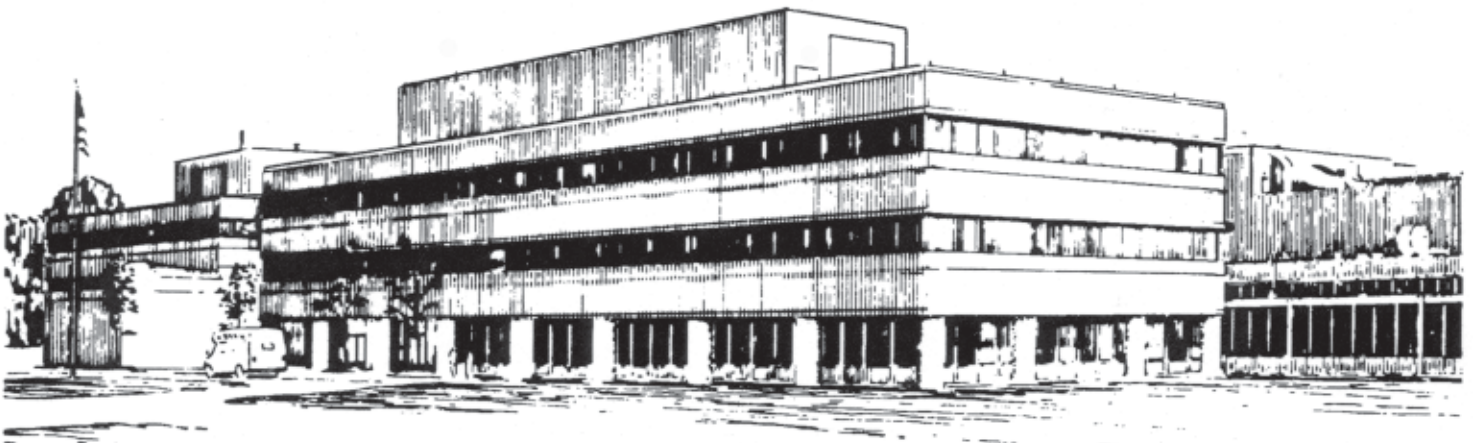
PPPL-3875

**Three-dimensional Neutral Transport Simulations
of Gas Puff Imaging Experiments**

by

D.P. Stotler, D.A. D'Ippolito, B. LeBlanc, R.J. Maqueda,
J.R. Myra, S.A. Sabbagh, and S.J. Zweben

September 2003



**PRINCETON PLASMA PHYSICS LABORATORY
PRINCETON UNIVERSITY, PRINCETON, NEW JERSEY**

PPPL Reports Disclaimer

This report was prepared as an account of work sponsored by an agency of the United States Government. Neither the United States Government nor any agency thereof, nor any of their employees, makes any warranty, express or implied, or assumes any legal liability or responsibility for the accuracy, completeness, or usefulness of any information, apparatus, product, or process disclosed, or represents that its use would not infringe privately owned rights. Reference herein to any specific commercial product, process, or service by trade name, trademark, manufacturer, or otherwise, does not necessarily constitute or imply its endorsement, recommendation, or favoring by the United States Government or any agency thereof. The views and opinions of authors expressed herein do not necessarily state or reflect those of the United States Government or any agency thereof.

Availability

This report is posted on the U.S. Department of Energy's Princeton Plasma Physics Laboratory Publications and Reports web site in Fiscal Year 2003. The home page for PPPL Reports and Publications is: http://www.pppl.gov/pub_report/

DOE and DOE Contractors can obtain copies of this report from:

U.S. Department of Energy
Office of Scientific and Technical Information
DOE Technical Information Services (DTIS)
P.O. Box 62
Oak Ridge, TN 37831

Telephone: (865) 576-8401

Fax: (865) 576-5728

Email: reports@adonis.osti.gov

This report is available to the general public from:

National Technical Information Service
U.S. Department of Commerce
5285 Port Royal Road
Springfield, VA 22161

Telephone: 1-800-553-6847 or
(703) 605-6000

Fax: (703) 321-8547

Internet: <http://www.ntis.gov/ordering.htm>

Three-Dimensional Neutral Transport Simulations of Gas Puff Imaging Experiments

D. P. Stotler^{*1}, D. A. D'Ippolito², B. LeBlanc¹, R. J. Maqueda³, J. R. Myra², S. A. Sabbagh⁴, and S. J. Zweben¹

¹ Princeton Plasma Physics Laboratory, Princeton University, P.O. Box 451, Princeton, NJ 08543-0451, USA

² Lodestar Research Corporation, Boulder CO 80301

³ Los Alamos National Laboratory, Los Alamos NM 87545

⁴ Dept. of Applied Physics and Applied Mathematics, Columbia Univ., NY, NY, 10027

Received 15 November 2003, revised 30 November 2003, accepted 2 December 2003

Published online 3 December 2003

Key words neutrals, simulation, plasma diagnostics

PACS 52.70.Kz, 52.25.Ya, 52.65.Pp, 52.55.Fa

Gas Puff Imaging (GPI) experiments are designed to isolate the structure of plasma turbulence in the plane perpendicular to the magnetic field. Three-dimensional aspects of this diagnostic technique as used on the National Spherical Torus eXperiment (NSTX) are examined via Monte Carlo neutral transport simulations. The radial width of the simulated GPI images are in rough agreement with observations. However, the simulated emission clouds are angled approximately 15° with respect to the experimental images. The simulations indicate that the finite extent of the gas puff along the viewing direction does not significantly degrade the radial resolution of the diagnostic. These simulations also yield effective neutral density data that can be used in an approximate attempt to infer 2-D electron density and temperature profiles from the experimental images.

Copyright line will be provided by the publisher

1 Introduction

The gas puff imaging (GPI) diagnostic [1, 2] is designed to provide high time resolution two-dimensional (2-D) data on plasma turbulence for comparison with three-dimensional (3-D) nonlinear plasma simulation codes, reduced theoretical turbulence models, and direct probe measurements of the turbulence. The technique consists of recording with high temporal and spatial resolution [1] light generated by neutral atoms puffed into the edge of the plasma.

The geometry used in the implementation of GPI on the National Spherical Torus Experiment (NSTX) [3] is designed to optimize the quality of the experimental data. However, the 3-D nature of the arrangement complicates interpretation of these experiments. Three-dimensional extensions of earlier DEGAS 2 [4] Monte Carlo neutral transport simulations of GPI experiments [2, 5] can aid in this task, e.g., by providing a quantitative assessment of the resolution of the diagnostic. Such simulations are described in Sec. 2. They are compared with experimental data in Sec. 3. An estimate of the diagnostic resolution is given in Sec. 4. Finally, in Sec. 5 we describe an approach to using these simulations to infer 2-D time-dependent plasma profiles from the GPI data. These plasma profiles can in turn be fed into a theory of blob transport [6, 7, 8], yielding predictions for the movement of coherent turbulent structures that can be quantitatively compared with observations.

2 Description of simulations

The helium gas puff in the NSTX GPI experiments [1] is produced by 30 holes in a 0.3 m straight tube tilted nearly perpendicular to the local magnetic field; the ideal result is a sheet of neutral gas entering the plasma. The camera viewing the 587.6 nm neutral helium emission line generated as this gas flows into the turbulent plasma is oriented perpendicular to this sheet (i.e., parallel to the magnetic field). The key assumption behind this arrangement, supported by extensive observations and theory [2], is that the plasma turbulence is extended along a field line, with much shorter scale lengths in the perpendicular directions.

The NSTX geometry used in DEGAS 2 begins with a simple outline of the vacuum vessel, including passive stabilizing plates. A 2-D plasma mesh based on an EFIT [9] equilibrium computed for the shot and time of interest is established using the DG [10] and CARRE [11] packages. The volume between the plasma mesh and the material surfaces is broken up into triangles [12]. The mesh zones in the emission region have linear dimensions on the order of a few millimeters.

* Corresponding author: e-mail: dstotler@pppl.gov, Phone: +1 609 243 2063, Fax: +1 609 243 2622

The geometry is divided into 3-D sections by planes of constant toroidal angle. The width of these sections is smallest, 0.5° to 1.0° , at the location of the gas puff and wider near the boundaries of the problem, 45° to either side of the manifold. The 3-D object representing the manifold is a vertical rectangle in the poloidal plane that is swept through an angle of 6° in the toroidal direction. The gas puff sources are specified along a line on the plasma-facing surface of this object that roughly mimics the 3-D shape of the actual gas manifold. To limit the computational size of the problem, only the volume between $R \simeq 1.1$ to 1.7 m and $Z \simeq -0.2$ to 0.6 m is treated.

The 81 by 161 pixel 2-D view provided by the GPI camera is simulated directly in DEGAS 2. The signal for each pixel is computed by integrating along a chord passing through the problem space. The starting point for all chords is the reentrant window through which the emission cloud is observed. We use data obtained from calibration of the GPI diagnostic to get a second point for each chord. Namely, during a machine opening, a physical plate was attached to the gas manifold and oriented perpendicular to the NSTX center stack. A measuring arm was used to physically locate on this “target plane” points made by back-lighting the optical system [1]. These measurements yielded the 3-D locations of the intersection of each chord with the target plane. The 0.4 cm resolution associated with each camera pixel is mocked up by treating each simulated chord as a cone of angular half-width 0.16° at the target plane.

Instantaneous midplane radial profiles of the plasma density and temperature are provided by a Thomson scattering system. The data are mapped onto the DEGAS 2 mesh by assuming that the electron and ion density and temperature are constant on a flux surface with $n_i = n_e$ and $T_i = T_e$. In the triangulated region of the computational mesh, the radial coordinate is estimated as the physical distance between the zone center and the nearest zone of the flux surface-based mesh. The simulations are time independent, suitable for comparison with time averaged GPI observations and with quiescent cases.

The collisional-radiative model developed by Goto [13] is used to describe the excitation and ionization of the puffed helium atoms. The metastable 2^1S and 2^3S states are not explicitly transported in these steady state simulations. Their role in time dependent situations will be examined in a subsequent paper. Elastic collisions between the helium atoms and the background deuterium ions are also included [14].

The emission rate of the 587.6 nm line (in $\text{m}^{-3}\text{s}^{-1}$) is computed by an expression equivalent to

$$S = n(1^1S) \frac{n(3^3D)}{n(1^1S)} A_{3^3D \rightarrow 2^3P} \equiv n_0 F(n_e, T_e), \quad (1)$$

where $n(1^1S)$ is the DEGAS 2 computed density of the electronic ground state atom; for notational simplicity, we will refer to this as n_0 . The ratio of the density of the upper state of the 587.6 nm transition to the ground state density, $n(3^3D)/n(1^1S)$, is provided by the collisional radiative model [13]. Its functional dependence on n_e and T_e , is described in [1] and [2]. The rate of spontaneous decay (Einstein coefficient) for the transition $A_{3^3D \rightarrow 2^3P} = 7.1 \times 10^7 \text{ s}^{-1}$. For convenience, we combine it and the density ratio into a single function, $F(n_e, T_e)$.

3 Comparison with Experiment

DEGAS 2 simulations have been performed of discharges 108311 (H-mode) and 108322 (L-mode); details of these discharges are in [2]. In both cases, the Thomson scattering data and EFIT equilibria closest in time to the GPI camera exposure have been used. The simulated camera images are shown in Figs. 1(a) and (b). The color map has been adjusted in both cases so that the cyan band is centered about half of the peak value.

The arrows in Fig. 1 indicate the physical radial and vertical directions. The core plasma is in the lower left of Fig. 1; the gas manifold is at the upper right. The imaged area is about 0.16 m wide and 0.32 m tall. As an additional orientation aid, note that the simulated contours align with constant n_e and T_e contours (i.e., flux surfaces) rather well. In physical space, the emission cloud is about 0.2 m above midplane; the flux surfaces there are 10° to 15° away from vertical.

The set of overlaid contours represents the corresponding GPI data. Since the Thomson scattering plasma data used in the DEGAS 2 simulations do not correspond to a particular GPI frame, we compare with a suitably averaged frame. A simple average of the available 28 frames is influenced noticeably by the passing of transient blobs [6, 7, 8]; we instead take the median over the 28 frames, reducing the impact of the blobs. The level of the middle of the three contours is half of the maximum.

The half-widths of the simulated emission clouds are 5 cm (108311) and 3 cm (108322). The range of observed widths found from the median and single frame images is 3 – 4 cm in 108311 and 3 – 5 cm in 108322. The level of agreement is noticeably better than that obtained with the earlier 2-D simulations [2, 15].

The experimental contours in Figs. 1 are angled roughly 15° with respect to the simulated images and, hence, with respect to flux surfaces and constant plasma contours. The apparent discrepancy between the emission cloud and separatrix positions has been noted previously [2]. A perusal of quiescent GPI data sets yields shot-to-shot variations in the observed emission cloud orientation of 20° . An examination of the EFIT equilibria from the discharges at the extremes of this range shows flux surface inclinations varying by only $1 - 2^\circ$, again indicating that the emission is not aligned with the flux surfaces. Since the GPI hardware has not been moved between these shots, the geometric calibration of the

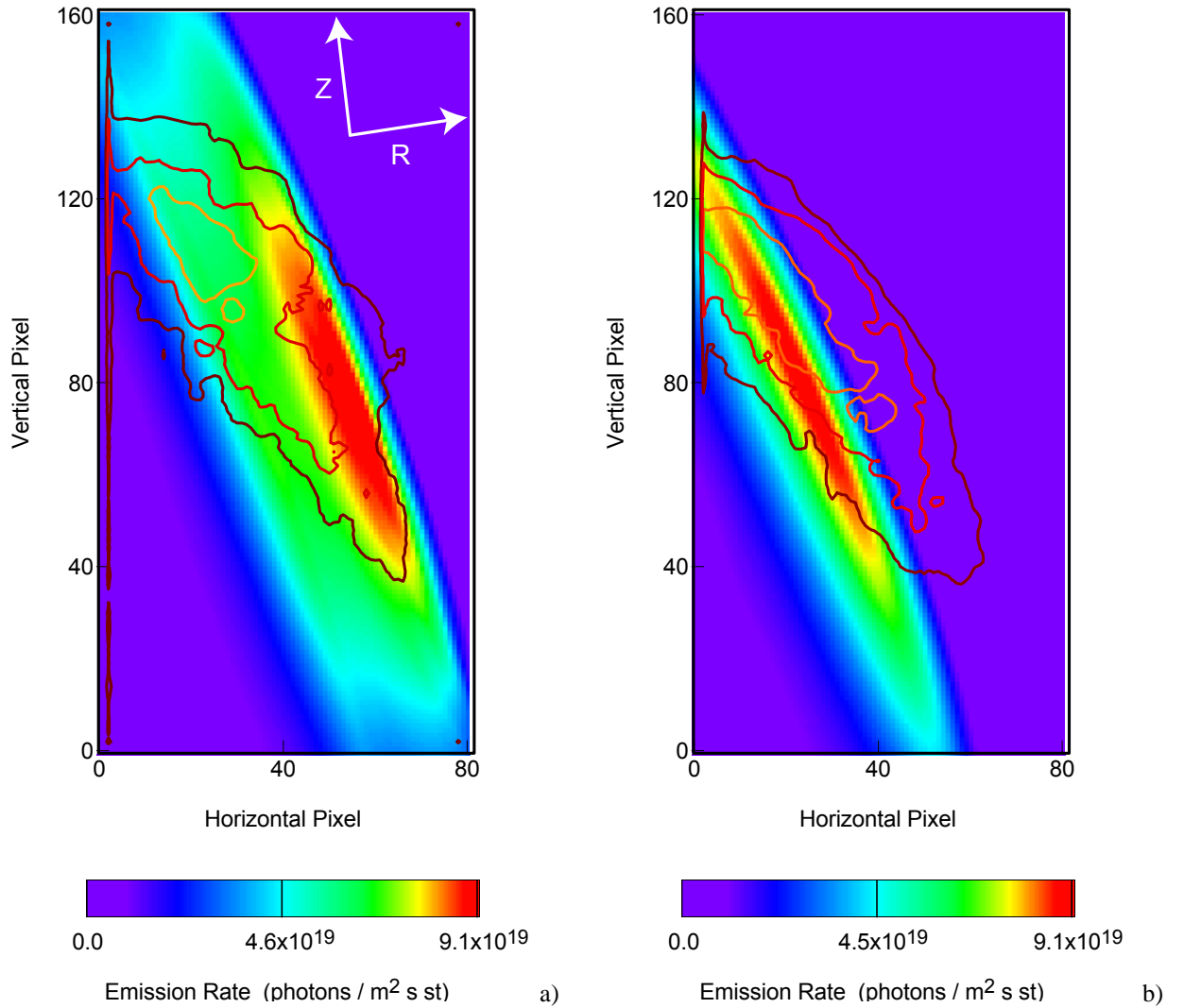


Fig. 1 Simulated (color images) and observed (line contours) camera data for NSTX shots 108311 (a) and 108322 (b). The experimental data are not absolutely calibrated. The simulations assume an experimentally relevant source rate of 6×10^{20} atoms / s [2]. The arrows in (a) indicate the directions of increasing major radius R and height above midplane Z .

diagnostic is not likely to blame for the discrepancy. Potential explanations include plasma parameters varying on flux surfaces and / or magnetic equilibrium shapes differing from those predicted by EFIT.

4 Radial Resolution Estimate

The radial resolution of the GPI diagnostic was previously estimated to be 2 ± 1 cm [1, 2] based on the observed width of the emission cloud along field lines and the degree of alignment between the camera viewing direction and the actual magnetic field lines. The effect of the latter on poloidal resolution was estimated to be 0.5 – 2 cm.

The 3-D DEGAS 2 simulations allow these estimates to be made more quantitative. We examine here only the impact of the toroidal extent of the emission cloud. The plasma current and magnetic field for shot 108322 are $I_p = 0.92$ MA and $B_T = 0.35$ T, roughly equal to the values assumed in the design of the GPI diagnostic, $I_p = 0.9$ MA, $B_T = 0.35$ T [1]. Hence, a different shot would have to be used to estimate the impact of field line misalignment on resolution; this will be addressed in a subsequent paper.

The width of the emission cloud along a field line can be quantified by taking 2-D slices through the simulated 3-D data that are aligned with the camera views. The resulting FWHM is 25 cm in the simulation of shot 108322 and 20 cm for shot 108311. Both values are in good agreement with the observed width of 24 cm [1].

We estimate the combined effect of the toroidally extended cloud and field line curvature on resolution by imposing a “tracer” perturbation on the plasma density. First, a single cell, about 0.7 cm wide and about 1 cm tall, is chosen from the 2-D poloidal mesh near the peak of the emission cloud. The toroidal discretization of the DEGAS 2 mesh for this run is then set up specifically to facilitate the definition of a field-line-following perturbation passing through this cell. Namely, the local magnetic field pitch is used to compute the change in toroidal angle associated with incremental

poloidal steps along the 2-D mesh on either side of the initial cell. When the plasma data are specified for this run, n_e is doubled everywhere along this path.

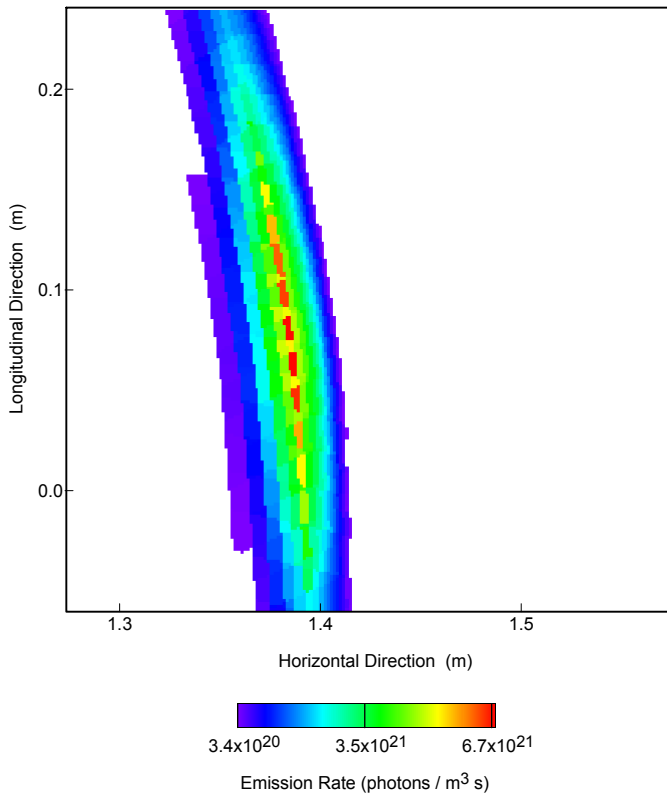


Fig. 2 Calculated emission rate in a 2-D slice aligned with the camera view at the vertical pixel corresponding to the location of the field-line-following n_e perturbation. The horizontal axis corresponds to the “horizontal pixel” direction in Fig. 1. The vertical axis represents distance along the viewing chord. The origin is chosen somewhat arbitrarily. In the plot coordinates, the camera is located at (1.56, -0.59). The yellow, orange, and red dashed line is the emission associated with the perturbation.

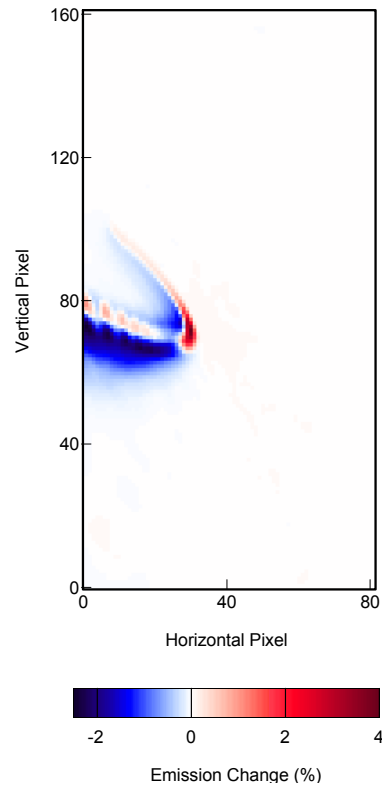


Fig. 3 Percent difference between camera images obtained with and without [Fig. 1(b)] a field-line-following n_e perturbation. The color map has been adjusted so that white corresponds to no difference between the two simulated images.

The resulting change in the emission is clearly apparent on the camera-aligned slice through the 3-D emission rate data as the dashed yellow, orange, and red line in Fig. 2. The plane of this slice is defined by the camera-viewing chord that passes through the initial cell described above. The relatively long length of the track in this plane is indicative of good alignment between the camera view and the path of the field line used to define the perturbation. The track is dashed because of the discrete nature of the computational mesh. The width of this track in the direction perpendicular to the viewing chord is about 1.6 cm, giving us a first measure of the radial resolution. However, the effective resolution is likely smaller since the camera signal is integrated along each viewing chord.

A more quantitative value for the resolution can be obtained by considering the impact of the perturbation on the camera image itself. The relative difference between the perturbed and unperturbed [Fig. 1(b)] camera images is shown in Fig. 3. The curved shape of the positive contours is indicative of the field line shape as seen by the camera. The negative values correspond to areas in the shadow [5] of the density perturbation relative to the gas manifold. The physical widths of the half-maximum contour of Fig. 3 are 0.6 cm radially and 1.2 cm poloidally, virtually identical to the dimensions of the initial cell in the poloidal plane. We conclude that the toroidal extent of the emission cloud does not significantly degrade the radial resolution, at least in this simulation.

5 Effective Neutral Density

Neutral density information from the DEGAS 2 simulations provides, via Eq. (1), a means for inferring time varying plasma profiles from the GPI data. The results can be used to directly characterize the plasma turbulence or to test theories of blob motion [6, 7, 8]. In these models, the 2-D spatial profiles of n_e and T_e determine the electric field and, hence, the $\vec{E} \times \vec{B}$ motion of plasma blobs. The GPI diagnostic essentially yields S in Eq. (1). Since the function $F(n_e, T_e)$ is known, the equation can be inverted if we can get n_0 from the DEGAS 2 simulations and we have some means of relating n_e to T_e [i.e., we know the function $n_e(T_e)$].

This process is complicated by the fact that the camera signal for pixel i is effectively a line integral of Eq. (1) along the viewing chord associated with that pixel,

$$I(i) = \int_i \frac{dl}{4\pi} F(\vec{x}) n_0(\vec{x}). \quad (2)$$

For brevity, we use i to represent one of the 2-D array of camera pixels. We get from the GPI diagnostic the emission rate as a function of i , yet we would like to find the corresponding plasma parameters as a function of \vec{x} . The only connection we have between the two spaces is the target plane (Sec. 2), where we know \vec{x}_i , the point at which it is crossed by chord i . So, the best result we can obtain is $n_e(\vec{x}_i)$ and $T_e(\vec{x}_i)$. To get at these values, we will consequently need to infer $F\{n_e(\vec{x}_i), T_e[n_e(\vec{x}_i)]\}$ from the experimental and simulation results.

Since the camera views are aligned with the magnetic field and the plasma perturbations are constant on field lines, F should be nearly constant along the line integral. We approximate its value as $F(\vec{x}_i)$. Then, Eq. (2) becomes

$$I(i) \simeq F(\vec{x}_i) \int_i \frac{dl}{4\pi} n_0(\vec{x}). \quad (3)$$

This expression suggests using

$$n_{0,\text{eff}} \equiv \int_i \frac{dl}{4\pi} n_0(\vec{x}) \simeq I(i)/F(\vec{x}_i). \quad (4)$$

The GPI data are not absolutely calibrated, so the simulated image needs to be normalized to the experimental data. Ideally, we would compute the required scaling factor by running DEGAS 2 with plasma profiles that correspond to an observed $I(i)$ image. However, we only have the single time point Thomson scattering profiles (Sec. 2). Assume that we have found some process (e.g., taking the median in time) that yields an experimental image consistent with the assumptions in the DEGAS 2 simulation. The needed scaling factor is just

$$\alpha \equiv I_e(i)/I_s(i), \quad (5)$$

where the subscript e (s) refers to “experimental” (“simulation”) data. To be useful, α must be a constant or only slightly varying with i .

Equation 4 can then be inverted for each frame k from the GPI camera, $I_e(i; t_k)$,

$$F(\vec{x}_i; t_k) = \frac{1}{\alpha} \frac{I_e(i; t_k)}{n_{0,\text{eff}}}. \quad (6)$$

This approach assumes that the transient passage of blobs does not significantly modify $n_{0,\text{eff}}$ and that the approximation in Eq. (4) is good.

Evaluations of Eq. (3) for shots 108311 and 108322 indicate, however, that the approximation made in Eq. (3) is not satisfactory, with an error of a factor a few that varies with i . A more accurate effective neutral density can be obtained by breaking Eq. (2) into two pieces,

$$I(i) = \int_{i;l \in l_0} \frac{dl}{4\pi} F(\vec{x}) n_0(\vec{x}) + \int_{i;l \notin l_0} \frac{dl}{4\pi} F(\vec{x}) n_0(\vec{x}), \quad (7)$$

where l_0 represents a portion of the chord within a specified distance of the target plane. We assume that the first integral is much larger than the second and define an average value of F ,

$$\langle F \rangle(i) \equiv \frac{\int_{i;l \in l_0} dl F(\vec{x}) n_0(\vec{x}) / 4\pi}{\int_{i;l \in l_0} dl n_0(\vec{x}) / 4\pi}. \quad (8)$$

A corresponding effective neutral density would then be

$$n'_{0,\text{eff}} \equiv I(i) / \langle F \rangle(i). \quad (9)$$

For sufficiently small l_0 , $\langle F \rangle \simeq F(\vec{x}_i)$ and the procedure described above for inverting the experimental $I(i; t)$ to obtain time-varying n_e profiles in the target plane still applies. Equation (9) does a better job of accounting for contributions to the integral away from the target plane than Eq. (3).

The value of l_0 must be large enough to encompass several computational zones to yield a spatially smooth $n'_{0,\text{eff}}$. The spatially noisy profiles obtained with smaller l_0 would hinder the attempt to infer n_e profiles from the experimental $I(i; t)$. However, if l_0 is too large, $\langle F \rangle$ no longer corresponds to $F(\vec{x}_i)$, and we cannot associate the inferred plasma data with the values at the target plane. In fact, note that Eqs. (4) and (9) are equivalent in the limit $l_0 \rightarrow \infty$.

The differences between simulated and observed emission clouds noted in Sec. 2 are currently large enough that the above considerations are secondary. The DEGAS 2 neutral densities must be shifted and rotated to achieve a satisfactory alignment between simulated and observed emission. In this case, Eqs. (4) and (9) work equally well.

Acknowledgements This work supported by US DOE contracts/grants DE-AC02-76CH03073, DE-FG03-02ER54678, DE-FG03-97ER54392, and W-7405-ENG-36.

References

- [1] R. J. Maqueda et al., *Rev. Sci. Instrum.* **74**, 2020 (2002).
- [2] S. J. Zweben et al., *Nucl. Fusion*, (2003) (to be published).
- [3] S. M. Kaye et al., *Phys. Plasmas* **8**, 1977 (2001).
- [4] D. P. Stotler and C. F. F. Karney, *Contrib. Plasma Phys.* **34**, 392 (1994).
- [5] D. P. Stotler et al., *J. Nucl. Mater.* **313–316**, 1066 (2003).
- [6] S. I. Krasheninnikov, *Phys. Lett. A* **283**, 368 (2001).
- [7] D. A. D'Ippolito et al., *Phys. Plasmas* **9**, 222 (2002).
- [8] D. A. D'Ippolito et al., *Contrib. Plasma Phys.*, (2003) (presented at this conference).
- [9] S. A. Sabbagh et al., *Nucl. Fusion* **41**, 1601 (2001).
- [10] D. P. Coster, 1999, private communication.
- [11] R. Marchand and M. Dumberry, *Comput. Phys. Comm.* **96**, 232 (1996).
- [12] J. R. Shewchuck, in: *Applied Computational Geometry: Towards Geometric Engineering*, Vol. 1148, edited by M. C. Lin and D. Manocha (Springer, New York, 1996), p. 203.
- [13] M. Goto, *J. Quant. Spectrosc. Radiat. Transfer* **76**, 331 (2003).
- [14] P. S. Krstic and D. R. Schultz, *J. Phys. B* **32**, 3485 (1999).
- [15] S. J. Zweben, et al., *Phys. Plasmas* **9**, 1981 (2002).

External Distribution

Plasma Research Laboratory, Australian National University, Australia
Professor I.R. Jones, Flinders University, Australia
Professor João Canalle, Instituto de Fisica DEQ/IF - UERJ, Brazil
Mr. Gerson O. Ludwig, Instituto Nacional de Pesquisas, Brazil
Dr. P.H. Sakanaka, Instituto Fisica, Brazil
The Librarian, Culham Laboratory, England
Mrs. S.A. Hutchinson, JET Library, England
Professor M.N. Bussac, Ecole Polytechnique, France
Librarian, Max-Planck-Institut für Plasmaphysik, Germany
Jolan Moldvai, Reports Library, Hungarian Academy of Sciences, Central Research Institute
for Physics, Hungary
Dr. P. Kaw, Institute for Plasma Research, India
Ms. P.J. Pathak, Librarian, Institute for Plasma Research, India
Ms. Clelia De Palo, Associazione EURATOM-ENEA, Italy
Dr. G. Grosso, Instituto di Fisica del Plasma, Italy
Librarian, Naka Fusion Research Establishment, JAERI, Japan
Library, Laboratory for Complex Energy Processes, Institute for Advanced Study,
Kyoto University, Japan
Research Information Center, National Institute for Fusion Science, Japan
Dr. O. Mitarai, Kyushu Tokai University, Japan
Dr. Jiengang Li, Institute of Plasma Physics, Chinese Academy of Sciences,
People's Republic of China
Professor Yuping Huo, School of Physical Science and Technology, People's Republic of China
Library, Academia Sinica, Institute of Plasma Physics, People's Republic of China
Librarian, Institute of Physics, Chinese Academy of Sciences, People's Republic of China
Dr. S. Mirnov, TRINITI, Troitsk, Russian Federation, Russia
Dr. V.S. Strelkov, Kurchatov Institute, Russian Federation, Russia
Professor Peter Lukac, Katedra Fyziky Plazmy MFF UK, Mlynska dolina F-2,
Komenskeho Univerzita, SK-842 15 Bratislava, Slovakia
Dr. G.S. Lee, Korea Basic Science Institute, South Korea
Institute for Plasma Research, University of Maryland, USA
Librarian, Fusion Energy Division, Oak Ridge National Laboratory, USA
Librarian, Institute of Fusion Studies, University of Texas, USA
Librarian, Magnetic Fusion Program, Lawrence Livermore National Laboratory, USA
Library, General Atomics, USA
Plasma Physics Group, Fusion Energy Research Program, University of California
at San Diego, USA
Plasma Physics Library, Columbia University, USA
Alkesh Punjabi, Center for Fusion Research and Training, Hampton University, USA
Dr. W.M. Stacey, Fusion Research Center, Georgia Institute of Technology, USA
Dr. John Willis, U.S. Department of Energy, Office of Fusion Energy Sciences, USA
Mr. Paul H. Wright, Indianapolis, Indiana, USA

The Princeton Plasma Physics Laboratory is operated
by Princeton University under contract
with the U.S. Department of Energy.

Information Services
Princeton Plasma Physics Laboratory
P.O. Box 451
Princeton, NJ 08543

Phone: 609-243-2750
Fax: 609-243-2751
e-mail: pppl_info@pppl.gov
Internet Address: <http://www.pppl.gov>